The Diurnal Temperature Range of the Middle Stratosphere

FREDERICK G. FINGER AND RAYMOND M. MCINTURFF

National Meteorological Center, Weather Bureau, ESSA, Hillcrest Hghts., Md.

(Manuscript received 24 May 1967, in revised form 1 April 1968)

ABSTRACT

An attempt is made to determine empirically the diurnal temperature range between 24 and 36 km, by using means of 12-hr temperature differences obtained from successive rawinsonde observations over North America. With a technique for isolating effects of solar radiation on the radiosonde instrument, it has become possible to construct a model of the middle stratospheric daily temperature variation. According to this model, the temperature reaches a maximum near sunset and a minimum near sunrise. The amplitude of the oscillation is found to increase with altitude between the 30- and 5-mb levels and to depend on latitude. A seasonal effect is strongly suggested.

1. Introduction

Attempts have been made to utilize radiosonde temperature data in a direct verification of theoretically derived values of the diurnal temperature variation at stratospheric levels. However, these have been hampered by limited knowledge concerning the total radiation error of the radiosonde instrument. It is well known that instrumental errors induced by solar radiation result in measured temperatures which, in the absence of other errors, are too high during daylight hours (Teweles and Finger, 1960). Infrared radiation from the earth-atmosphere system (hereafter referred to simply as infrared or longwave radiation) also causes errors in measurement, with a tendency to lower the values of reported temperatures by increasing amounts with increasing height above about 24 km (Barr, 1961).

Several studies have attempted to circumvent the inherent radiation error of the radiosonde thermistor by employing wind observations in an independent method of computing temperature variations (Harris, 1959; Harris *et al.*, 1962; Finger *et al.*, 1965a). These have made use of a rather restrictive model based on a linearized form of the equations of motion with the assumptions that the flow is frictionless and that the oscillations are simple progressive waves. The values of the variations computed from wind observations are in general agreement with earlier calculations of the diurnal temperature variation based on radiative equilibrium considerations, but differ considerably from those computed directly from temperature observations.

Day-night temperature differences computed from reported rawinsonde data have been used to show the existence of solar radiation errors at levels of 100 mb and above (Teweles, 1963; Finger *et al.*, 1964). This has been accomplished by analyzing large samples of temperature data, which show a functional dependence of 12-hr day-night differences upon the daytime solar elevation angle (the angle being computed for the time the daylight observation is taken at a given pressure surface). Matters are complicated by the fact that the day-night differences also contain the component of change induced by the real diurnal temperature variation.

Separation of the various components of the day-night temperature change (solar radiation error, infrared radiation error, and real diurnal temperature change) might be possible if 12-hr differences could be computed from standard observations (0000 and 1200 GMT) that are both in daylight (double-daylight) or both in darkness (double-darkness). For example, if the length of day were such that one observation could be taken in morning daylight and the other (12 hr later) in afternoon daylight, and if the solar angle were the same at both times, the error due to solar radiation (though not necessarily that due to terrestrial radiation) should be subtracted out in the computation of temperature differences. Solar error need not be considered, of course, when both observations are taken during nighttime hours, but longwave radiation error must still be considered.

With a method for eliminating the effects of instrumental error, 12-hr differences of temperature from successive observations taken in either double-darkness or double-daylight might be used to derive a model of the real diurnal temperature oscillation.[1] It is the purpose of this paper to report on the results of analyzing a large sample of radiosonde data in an attempt to construct such a model. In addition to double-darkness and double-daylight observations, those taken consecutively in daylight and darkness will also be used. The atmospheric levels selected for study are 30, 10 and 5 mb.

[1] The terms "diurnal" and "daily" will be used interchangeably to refer to the composite variation, since no harmonic analysis has been performed.

2. Data source

The question arises as to how the required data (from successive rawinsonde observations, both taken in daylight or both in darkness at stratospheric levels) mentioned above can be obtained. Actually, there are two areas in the Northern Hemisphere where, according to season, both observations may be taken in darkness (double-darkness) or daylight (double-daylight). In addition, at certain times of the year, one observation may be taken in daylight and the other in darkness. The areas are centered about 90° of longitude east and west of the zero meridian, in North America and in Central Asia.

A clear view of the daylight-darkness areas over North America with respect to the 1200 and 0000 GMT observations and the 30-mb level can be obtained from

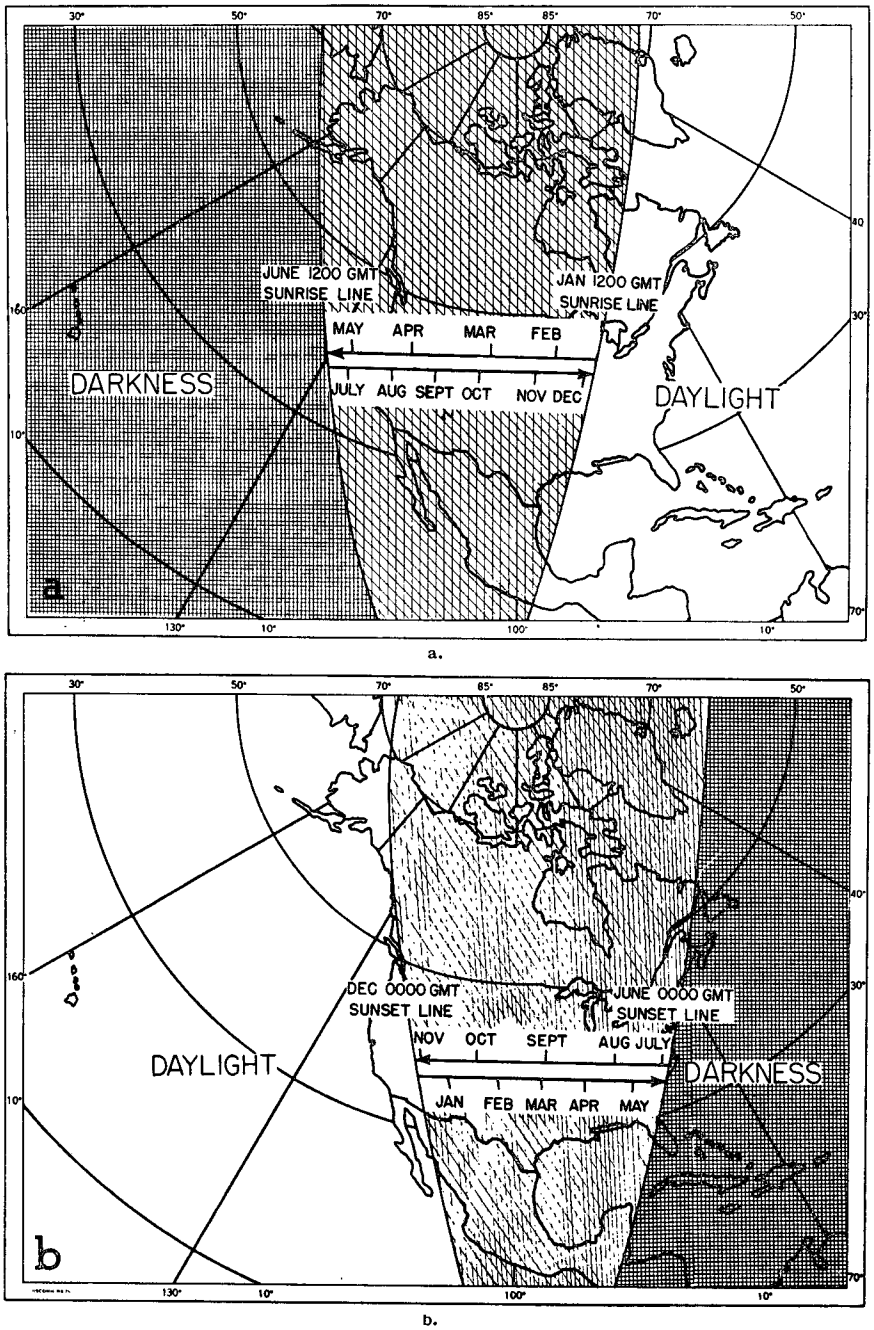

FIG. 1. Yearly migration of 1200 GMT sunrise line, a., and 0000 GMT sunset line, b., at 30 mb (from Finger *et al.*, 1964). Direction of movement during period between extremes is shown by arrows. Position of line on the 15th day of each month is indicated by small line segments showing the general orientation of the line.

at 1130 GMT for the 1200 GMT run) reach the 30-mb level in daylight east of the line through the western Great Lakes down into the western Gulf of Mexico. West of this line, there is still darkness as the balloon passes through 30 mb. As can be seen, the daylight-darkness line migrates westward from January to a position in the eastern Pacific in June, thence beginning a return eastward. A similar explanation can be given for the 30-mb, 0000 GMT daylight-darkness line. A close inspection of Fig. 1 will reveal that both the 1200 and 0000 GMT observations are taken in darkness at 30 mb during the winter and in daylight during the summer over a large portion of North America. During the equinoctial periods, the 1200 GMT observation is in daylight over eastern North America while that for 0000 GMT is in darkness. The reverse is true of western North America with the 0000 GMT observation in daylight and that for 1200 GMT in darkness.

The data sample used for this study includes mainly 30- and 10-mb temperatures reported from January 1964 through June 1966 by all stations in North America which employ the ESSA Weather Bureau outrigger type radiosonde instrument. These stations are located in the contiguous United States, Alaska and Canada. Punched card decks containing reported temperature data for all these stations have been produced at the National Meteorological Center on a daily basis since January 1964. These decks are a by-product of a computerized analysis system devised for the construction of a daily Northern Hemisphere map series at the 100-, 50-, 30- and 10-mb levels (Finger *et al.*, 1965b). Also included on the cards is an indication of the solar elevation angle as a function of observation time and of stratospheric level. The solar angle is a very important parameter for this study, as will be evident later. Data for 5-mb computations covering the period from January 1964 through December 1965 were obtained from the National Weather Records Center. (The 5-mb data include those obtained at Thule, Greenland, by means of the U. S. military outrigger radiosonde.)

The 12-hr temperature difference computations used for this study were previously designed and computer-processed in connection with a large-scale effort to insure compatibility of reported temperatures between stations in the Northern Hemisphere which use various types of radiosonde instruments. (This compatibility procedure greatly aids the objective analysis of constant-pressure charts.) The computations were accomplished by the simple relation

$$\overline{\Delta T}=-\frac{1}{n}\sum_{i=1}^{n}[T(00)-T(12)]_i,$$

where $\overline{\Delta T}$ represents a monthly average, $T(00)$ and $T(12)$ are temperatures observed at 0000 and 1200 GMT, respectively, and n is the total number of differences for the month in question (referred to hereafter as the d number) at each station. Differences were computed for both the 12 hr preceding and the 12 hr following 0000 GMT, not only to obtain as many differences as possible, but also, and more importantly, in order to minimize the effects of certain weather trends. The program also calculated the 0000 and 1200 GMT monthly mean solar elevation angles. These angles were computed for both daytime and nighttime observations with respect to a point on the earth's surface (negative angles with respect to the earth's surface may occur even when daylight persists at 30 mb and above).

The pre-processed data used for the study fall into three distinct categories:

1) Monthly means of temperature differences between successive 0000 and 1200 GMT observations taken during daylight hours. Each such mean for a given station will be designated as $(\overline{\Delta T})_D$. To qualify for the double-daylight category, the monthly mean solar angles $\overline{\alpha(00)}$ and $\overline{\alpha(12)}$ for the 0000 and 1200 GMT observations, respectively (the angle for a given observation is used for computation of the monthly mean only if the temperature is available), must exceed $-5.6°$ at 30 mb, $-6.0°$ at 10 mb, and $-7.0°$ at 5 mb.

2) Monthly means $(\overline{\Delta T})_N$ of temperature differences between successive 0000 and 1200 GMT observations taken during nighttime hours. For double-darkness, the monthly mean solar angles for both observations must be less than values given in 1) above.

3) Monthly means of temperature differences between successive 0000 and 1200 GMT observations, one of which is taken in daylight and the other in darkness. In order to be included in this category, either the 0000 or 1200 GMT observation must be taken with a solar angle exceeding $-5.6°$ at 30 mb. $-6.0°$ at 10 mb, and $-7.0°$ at 5 mb, while the other (the previous or subsequent) is taken with angles less than those stated.

3. Plotting and analysis of data

In order to obtain two-dimensional graphical representations of $(\overline{\Delta T})_D$ and $(\overline{\Delta T})_N$ as functions of the mean solar elevation angles $\overline{\alpha(00)}$ and $\overline{\alpha(12)}$, the abscissas have been chosen as $\overline{\alpha(12)}-\overline{\alpha(00)}$, also denoted as $\Delta\bar{\alpha}$. It can be seen that the time order used in computing $\Delta\bar{\alpha}$ is different from that used in computing $\overline{\Delta T}$; this facilitates interpretation of the graphs.

Since the data sample was large, and theoretical studies have indicated a latitudinal dependency of the true diurnal variation (Pressman, 1955; Leovy, 1964), the data were categorized according to latitudinal band. Figs. 2–10 are examples of the graphs at the 30-, 10- and 5-mb levels for several latitudinal bands. The sample was not suitable for an investigation of possible longitudinal variations.

An interpretation of the abscissas in Figs. 2–10 can be made by reference to Figs. 1 and 11. In midsummer,

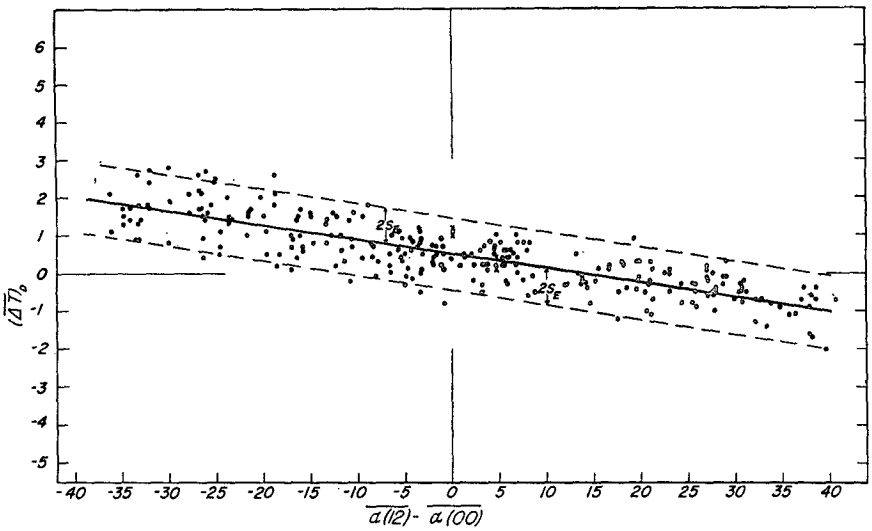

FIG. 2. Double-daylight $\overline{\Delta T}$ vs $\Delta\bar{\alpha}$ scatter diagram for 30 mb, 40–50N. Cross marks represent values of $\overline{\Delta T}$ corresponding to differences between low solar angles (both $<5°$); closed circles represent all others. The dashed lines enclose points within 2 standard estimates of error s_E of the fitted straight line. Units of ordinate are °C, units of abscissa degrees of angular measure.

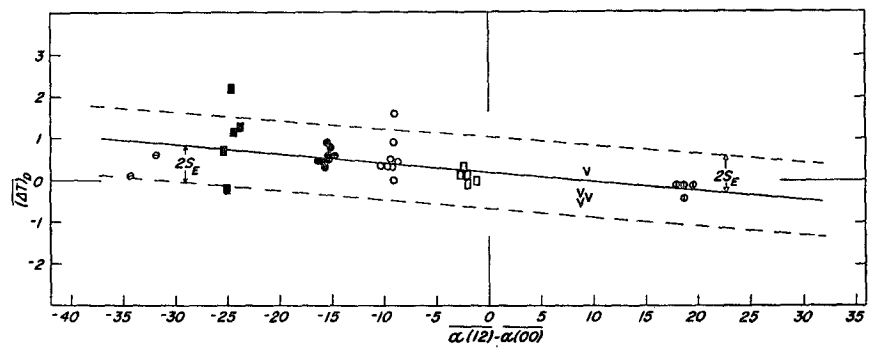

FIG. 3. Double-daylight $\overline{\Delta T}$ vs $\Delta\bar{\alpha}$ scatter diagram for 30 mb, 70–80N. [The clusters of various symbols represent reporting stations distributed geographically from west (left) to to east (right).] Units as in Fig. 2.

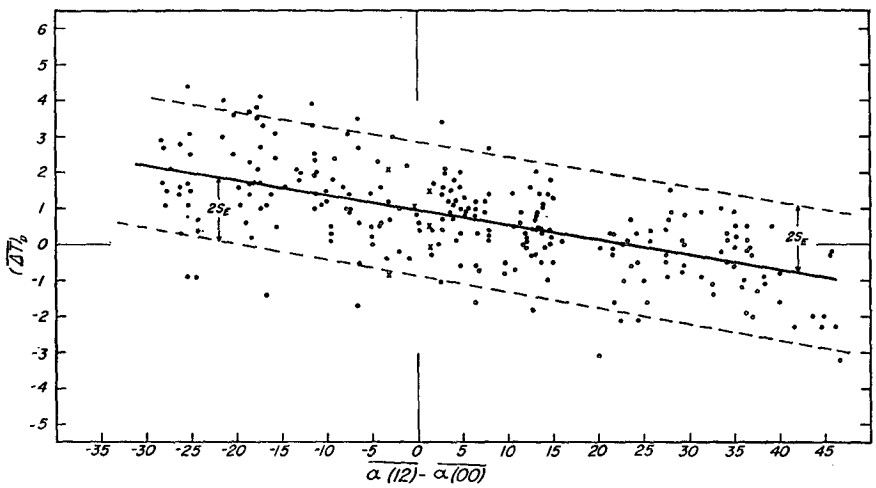

FIG. 4. Double-daylight $\overline{\Delta T}$ vs $\Delta\bar{\alpha}$ scatter diagram for 10 mb, 40–50N. Explanation as in Fig. 2.

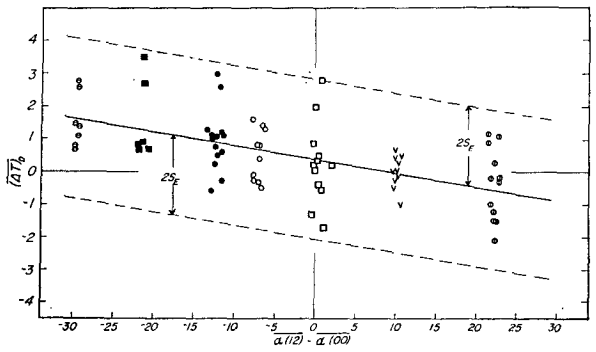

FIG. 5. Double-daylight $\overline{\Delta T}$ vs $\Delta\bar{\alpha}$ scatter diagram for 10 mb, 70–80N. Explanation as in Fig. 3.

for example, it is evident from Fig. 1 that practically all of North America is in daylight at the times that both the 0000 and 1200 GMT observations reach 30 mb. Fig. 11 illustrates the range of $\Delta\bar{\alpha}$ for the 30-mb level during the month of July. The zero line near the middle of the continent indicates the solar angle is equal for both the 0000 and 1200 GMT observations. To the east of zero, the solar angle at 1200 GMT is higher by the amount indicated. The reverse is true to the west of zero, with the 0000 GMT angles higher.

It is important to observe that the angles $\alpha(12)$ and $\alpha(00)$ for which $\alpha(12)\cong\alpha(00)$ are never high angles. At the time of the equinoxes, these angles are very low (occurring at times near sunrise and sunset). Both of

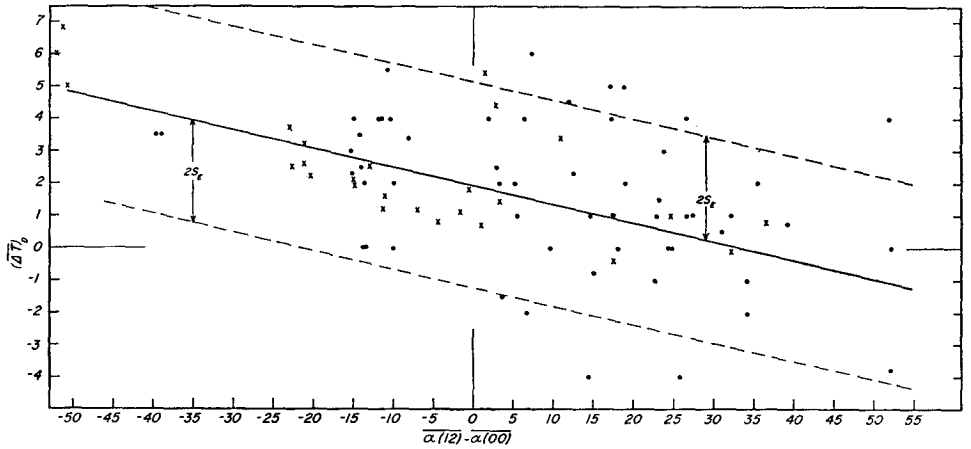

FIG. 6. Double-daylight $\overline{\Delta T}$ vs $\Delta\bar{\alpha}$ scatter diagram for 5 mb, 30–60N. Each cross mark represents a $\overline{\Delta T}$ derived from a d number >5, the dots being based on samples of smaller d numbers. Units as in Fig. 2.

the angles reach a maximum at the summer solstice. Near 45N, daylight extends through about 16 hr in midsummer, so that $\alpha(00)$ would occur 2 hr before sunset and $\alpha(12)$ 2 hr after sunrise (each solar angle would be approximately 17°).

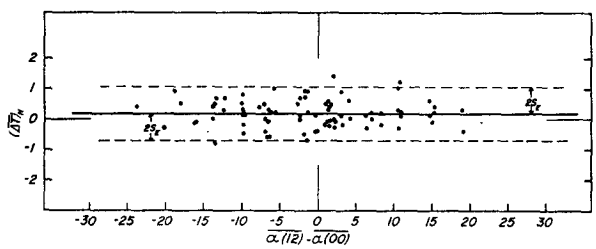

FIG. 7. Double-darkness $\overline{\Delta T}$ vs $\Delta\bar{\alpha}$ scatter diagram for 30 mb, 40–50N. Units as in Fig. 2.

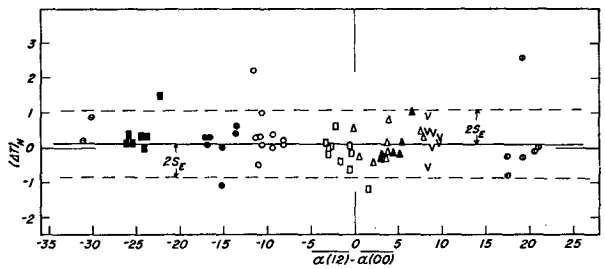

FIG. 8. Double-darkness $\overline{\Delta T}$ vs $\Delta\bar{\alpha}$ scatter diagram for 30 mb, 70–80N. Explanation as in Fig. 3.

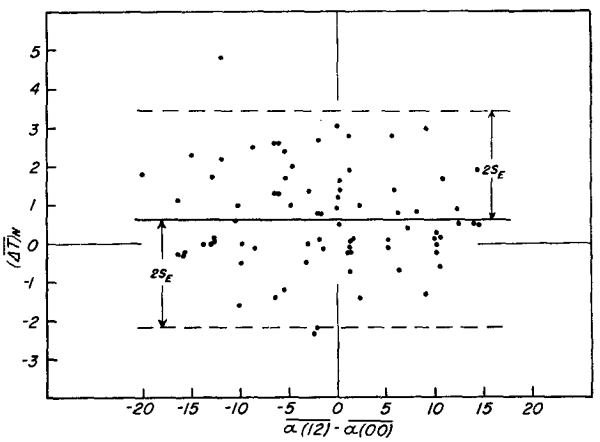

FIG. 9. Double-darkness $\overline{\Delta T}$ vs $\Delta\bar{\alpha}$ scatter diagram for 10 mb 40–50N. Units as in Fig. 2.

The constantly shifting sunrise and sunset lines (Fig. 1) also may be employed to delineate the limited area within North America where both rawinsonde observations occur during darkness hours in winter. Since this area is considerably smaller than that for double-daylight in summer, the range of $\Delta\bar{\alpha}$ shown in the double-darkness diagrams (Fig. 7–10) is relatively restricted.

A method of least squares was employed for the analysis of the $\overline{\Delta T}$ vs $\Delta\bar{\alpha}$ diagrams. Each monthly mean temperature difference $\overline{\Delta T}$ was weighted with respect to its d number. A total of 22 scatter diagrams were analyzed, with the latitudinal bands and magnitudes of data samples (sums of d numbers, each denoted by the symbol n) shown in Tables 1 (summer) and 2 (winter). Sparsity of data limited the analysis at 5 mb to the double-daylight category at two latitudinal bands. The slopes derived from the analyses are given as $\hat{m}$, while the y intercepts (ordinate values corresponding to the zero abscissas) are given as $\hat{b}$. The corresponding population parameters are denoted by m and b, respectively, and their 95% confidence intervals are listed. The standard errors s_E about the regression are also given.

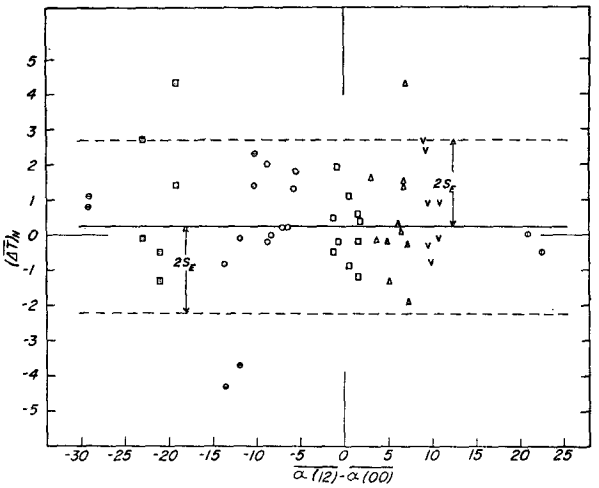

FIG. 10. Double-darkness $\overline{\Delta T}$ vs $\Delta\bar{\alpha}$ scatter diagram for 10 mb, 70–80N. Explanation as in Fig. 3.

4. Discussion of scatter diagrams

Since other studies have shown that the solar error is a direct function of the daytime elevation angle of the sun (Teweles, 1963; Finger *et al.*, 1964), it appears that

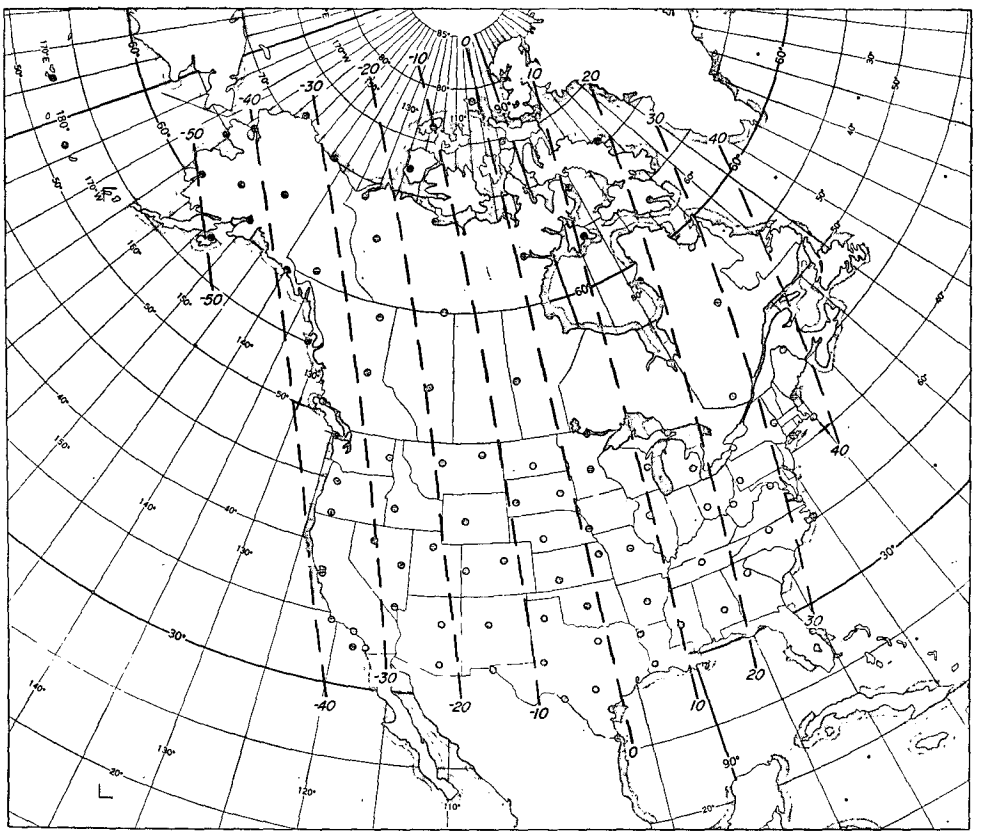

FIG. 11. Distribution of North American upper air stations which have provided double-daylight data for July 1964. The geographical distribution corresponds to the distribution of $\overline{\alpha(12)}-\overline{\alpha(00)}$ values, indicated by the dashed curves, which are labeled in degrees of angle differences.

TABLE 1. Statistics for the double-daylight $\overline{\Delta T}$ vs $\Delta\bar{\alpha}$ scatter diagrams.

Scatter diagram Level	Latitude	n	$\hat{m}$	95% confidence intervals	$\hat{b}$	95% confidence intervals	s_E
30 mb	30–40N	9711	−0.036	$-0.040 \leqslant m \leqslant -0.032$	0.484	$0.477 \leqslant b \leqslant 0.491$	0.63
30 mb	40–50N	9102	−0.038	$-0.041 \leqslant m \leqslant -0.035$	0.500	$0.492 \leqslant b \leqslant 0.508$	0.49
30 mb	50–60N	4859	−0.026	$-0.029 \leqslant m \leqslant -0.023$	0.340	$0.335 \leqslant b \leqslant 0.345$	0.43
30 mb	60–70N	6621	−0.026	$-0.029 \leqslant m \leqslant -0.023$	0.203	$0.173 \leqslant b \leqslant 0.233$	0.38
30 mb	70–80N	4021	−0.027	$-0.031 \leqslant m \leqslant -0.023$	0.179	$0.170 \leqslant b \leqslant 0.188$	0.33
10 mb	30–40N	7642	−0.043	$-0.051 \leqslant m \leqslant -0.035$	1.005	$0.940 \leqslant b \leqslant 1.070$	1.17
10 mb	40–50N	6041	−0.041	$-0.047 \leqslant m \leqslant -0.035$	0.952	$0.903 \leqslant b \leqslant 1.001$	0.97
10 mb	50–60N	2879	−0.041	$-0.048 \leqslant m \leqslant -0.034$	0.723	$0.680 \leqslant b \leqslant 0.766$	1.04
10 mb	60–70N	3239	−0.024	$-0.031 \leqslant m \leqslant -0.017$	0.471	$0.396 \leqslant b \leqslant 0.546$	1.01
10 mb	70–80N	2069	−0.037	$-0.049 \leqslant m \leqslant -0.026$	0.347	$0.343 \leqslant b \leqslant 0.351$	0.86
5 mb	30–60N	400	−0.058	$-0.073 \leqslant m \leqslant -0.043$	1.946	$1.846 \leqslant b \leqslant 2.046$	1.58
5 mb	60–80N	117	−0.044	$-0.075 \leqslant m \leqslant -0.013$	1.322	$0.875 \leqslant b \leqslant 1.769$	1.50

TABLE 2. Statistics for the double-darkness $\overline{\Delta T}$ vs $\Delta\bar{\alpha}$ scatter diagrams.

Scatter diagram Level	Latitude	n	$\hat{m}$	95% confidence intervals	$\hat{b}$	95% confidence intervals	s_E
30 mb	30–40N	3045	−0.005	$-0.018 \leqslant m \leqslant 0.008$	0.333	$0.330 \leqslant b \leqslant 0.336$	0.44
30 mb	40–50N	2795	0.003	$-0.007 \leqslant m \leqslant 0.013$	0.178	$0.169 \leqslant b \leqslant 0.187$	0.44
30 mb	50–60N	2206	−0.001	$-0.009 \leqslant m \leqslant 0.007$	0.253	$0.246 \leqslant b \leqslant 0.260$	0.46
30 mb	60–70N	1659	−0.010	$-0.018 \leqslant m \leqslant -0.002$	0.201	$0.168 \leqslant b \leqslant 0.234$	0.47
30 mb	70–80N	2067	−0.008	$-0.017 \leqslant m \leqslant 0.001$	0.077	$0.038 \leqslant b \leqslant 0.116$	0.48
10 mb	30–40N	1793	−0.047	$-0.082 \leqslant m \leqslant -0.012$	0.438	$0.408 \leqslant b \leqslant 0.468$	1.09
10 mb	40–50N	1377	−0.016	$-0.048 \leqslant m \leqslant 0.016$	0.593	$0.559 \leqslant b \leqslant 0.627$	1.24
10 mb	50–60N	641	0.004	$-0.033 \leqslant m \leqslant 0.041$	0.736	$0.563 \leqslant b \leqslant 0.909$	1.53
10 mb	60–70N	837	−0.011	$-0.041 \leqslant m \leqslant 0.019$	0.134	$0.116 \leqslant b \leqslant 0.152$	1.89
10 mb	70–80N	1073	−0.018	$-0.044 \leqslant m \leqslant 0.008$	0.230	$0.180 \leqslant b \leqslant 0.280$	1.04

the slopes of the double-daylight analyses are primarily the result of instrumental, solar radiation error. Thus, the mean temperature differences $(\overline{\Delta T})_D$ for daytime observations vary according to differences of corresponding mean angles [i.e., according to $\overline{\alpha(12)}-\overline{\alpha(00)}$]. The slopes of the lines exhibit a general increase in absolute value with altitude. For the levels of interest in this paper, solar radiation error is heavily dependent on atmospheric density, i.e., the error increases with decreasing density. According to C. Harmantas,[2] although the solar radiation input remains fairly constant with height at the levels of concern, the heat dissipation from the instrument decreases with decreasing density.

In contrast to the double-daylight diagrams, those obtained from double-darkness observations display only insignificant slopes. This can be seen in Table 2, which shows that for these diagrams one cannot reject the hypothesis of zero slope at the 95% confidence level (with only two exceptions). It is for this reason that zero slope is indicated in Figs. 7–10.

Any variability of infrared radiative effect on the instrument from the earth and atmosphere should be most clearly evident in the double-darkness analyses, since there is no direct solar radiation to obscure it. Several studies (Badgley, 1957; Barr, 1961; Ney *et al.*, 1961) have shown (for the levels involved in the present study) that, in the absence of other errors, this infrared radiative effect would result in reported temperatures that are lower than the actual temperatures of the ambient air.

According to more recent studies (Rao *et al.*, 1965; Kuhn and Cox, 1968), the infrared radiation from the earth-atmosphere system exhibits a rather complex variation, but to a first approximation may be considered constant throughout darkness and daylight at the levels of present concern. In view of this, the values of $\hat{b}$ assume special importance, because they provide measures of 12-hr temperature changes independent of infrared radiation error.

On each of the double-daylight graphs, $\hat{b}$ represents an average 12-hr temperature change between times in morning and afternoon when the solar elevation angles are equal, i.e., $\alpha(00)=\alpha(12)$. With solar error expressed as $T(\alpha)$, a function of solar elevation angle, we have (neglecting other possible sources of error), for T_a the true afternoon temperature, T_m the true morning temperature and T_i a constant infrared error, $\hat{b}=T(00)-T(12)=[T_a+T_i+T(\alpha)]-[T_m+T_i+T(\alpha)]=T_a-T_m$. In other words, the effect of solar error is removed for $\alpha(00)=\alpha(12)$, and the quantity T_i is eliminated. As will be seen in Section 6, this is especially significant for determination of the diurnal temperature range.

On each of the double-darkness graphs, the analysis can be closely represented as $y=\hat{b}$(constant). Thus, the value of the ordinate approximates a true 12-hr temperature change, $T(00)$ being invariably greater than

[2] Private communication.

$T(12)$ because there is no error due to solar radiation, and the constancy of the infrared error T_i entails its elimination upon taking differences; thus,

$$\hat{b}=T(00)-T(12)=(T_a+T_i)-(T_m+T_i)=T_a-T_m.$$

In what follows, it will become apparent that the analysis of all the scatter diagrams has been performed with just one end in view: the determination of $\hat{b}$ and its statistical significance. The physical interpretation of $\hat{b}$ will be given in the following sections. It should be noted here, however (with reference to Table 1), that $\hat{b}$ for double-daylight tends (at any given pressure level) to decrease with increasing latitude, while it tends (at any given latitude)to increase with increasing altitude. The behavior of $\hat{b}$ for double-darkness (Table 2) is more complex.

5. Day-night temperature differences

As indicated earlier, additional information was available, involving a large number of 12-hr day-night differences. These monthly mean differences were computed for stations in North America, primarily the same stations utilized for the double-daylight and double-darkness graphs. Reference to Fig. 1 reveals that during spring and autumn the majority of stations take one standard observation in darkness and the other in daylight. It is important to note that in western North America the daylight observation during these periods is always 0000 GMT, which corresponds to middle and late afternoon hours. In the east, the daylight observation at 1200 GMT takes place during morning hours.

The curves in Fig. 12 show the results of 10-mb, monthly mean, day-night difference analyses (for North America) as functions of the mean solar elevation angles of the daylight reports. Most striking are the larger ΔT values exhibited by the afternoon daylight stations for the same solar angles as the morning daylight stations. Further, the data clearly indicate that early morning daylight temperatures are lower than those reported in darkness immediately after sunset.

Perhaps the most important point to be made is that the vertical distance between the two day-night difference curves (i.e., for a given solar elevation angle) is a function of the diurnal temperature range exclusively (since the radiation error is the same whenever the solar elevation angle is the same).

6. Model of daily temperature variation in the stratosphere

It becomes possible, with the aid of the double-daylight, double-darkness, and day-night temperature differences, to estimate the magnitude of the real diurnal temperature variation. A model will be presented, showing what is thought to be a reasonable picture of the real and spurious temperature variations at the 10-mb level at 45N. A complicating factor in determining the

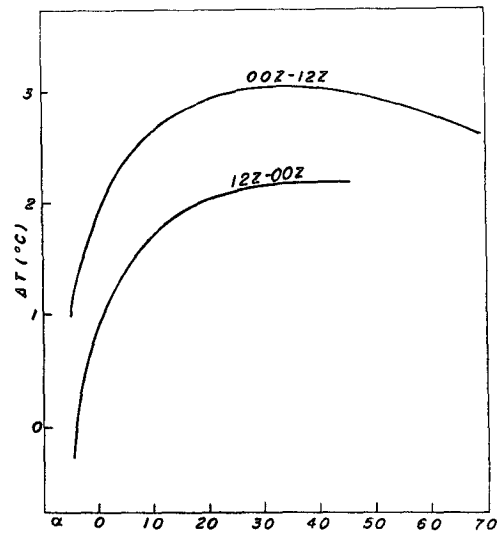

FIG. 12. Monthly mean 12-hr day-night temperature differences vs monthly mean solar angles (of daylight observations) over North America, at 10 mb. Upper curve represents afternoon-night differences, lower curve represents morning-night differences.

true variation is the seasonal representativeness of the data samples used in the study. As already stated, the double-daylight results are keyed to the summer season, while those for double-darkness represent wintertime conditions. Therefore, the model will have two distinct parts, one corresponding to summer and one to winter. The day-night differences will be used as an aid in constructing the two parts.

Since all of the double-daylight information was obtained between the vernal and autumnal equinoxes, a day in the middle of May (equivalently, mid-August) was selected to depict "average" conditions of length of day and solar angle for the summer section of the model (Fig. 13). At this time, the solar elevation angle at 45N reaches approximately 63° at local noon. The entire day is represented in the model; therefore, the abscissa shows the solar angle α, which is about $-7°$ at the 10-mb level when sunrise and sunset (abbreviated as SR and SS) occur, rising to a peak of 63° from sunrise to noon, thence decreasing to sunset. A linear time scale (top) corresponds to the solar angles. A similar scale was derived for the wintertime section of the model (Fig. 14), where daylight at the 10-mb level is restricted to less than 12 hr.

As stated earlier, $\hat{b}$ (defined as the ordinate value corresponding to the zero abscissa on each of the scatter diagrams, Figs. 2–10) is an average of real temperature differences derived from pairs of observations, one member of each pair being taken near sunrise, the other near sunset. Since the diurnal curve is periodic, and, according to convention, is shown as a set of departures from a horizontal line representing the daily mean, it is convenient to place the zero axis of the model in such a way that the temperature is shown increasing from a value $-0.5\hat{b}$ near sunrise to a value $+0.5\hat{b}$ near sunset. The

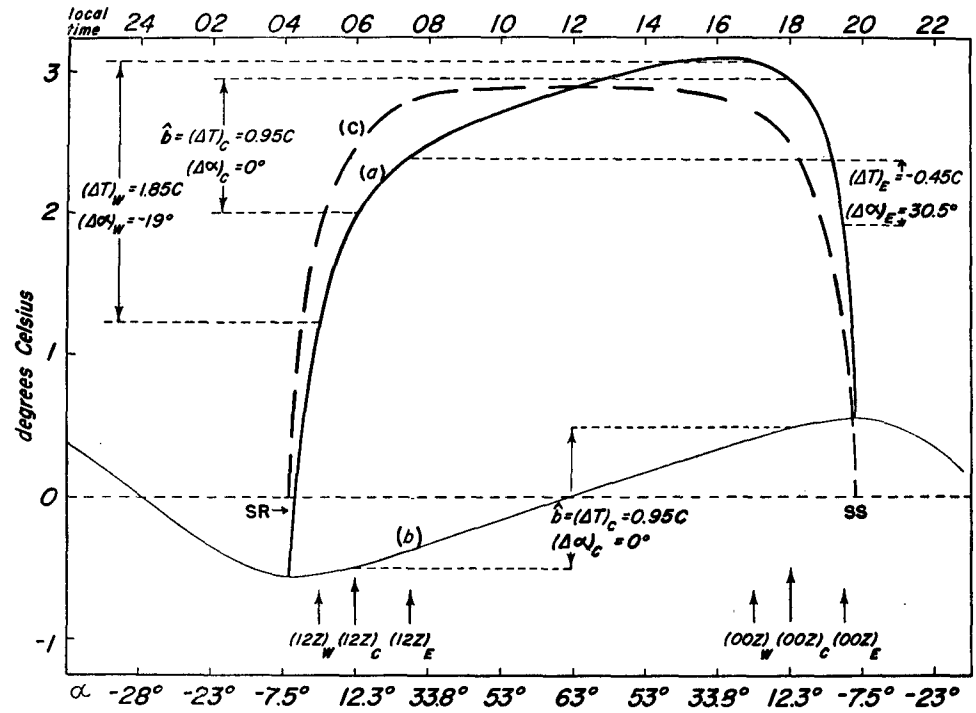

FIG. 13. Model of summertime temperature variation for 10 mb, 45N.

$\hat{b}$ values (one for summer, the other for winter—Figs. 13 and 14, respectively) thus provide two points on each of the 24-hr diurnal curves (b), without, however, giving any indication of the shape of the curve, or the phase of the oscillation.

Placing the zero horizontal axis of Figs. 13 and 14 in such a manner with respect to the diurnal curve (b) can be justified only on the ground that it represents the mean daily temperature. The two points of the diurnal curve discussed in the preceding paragraph are then

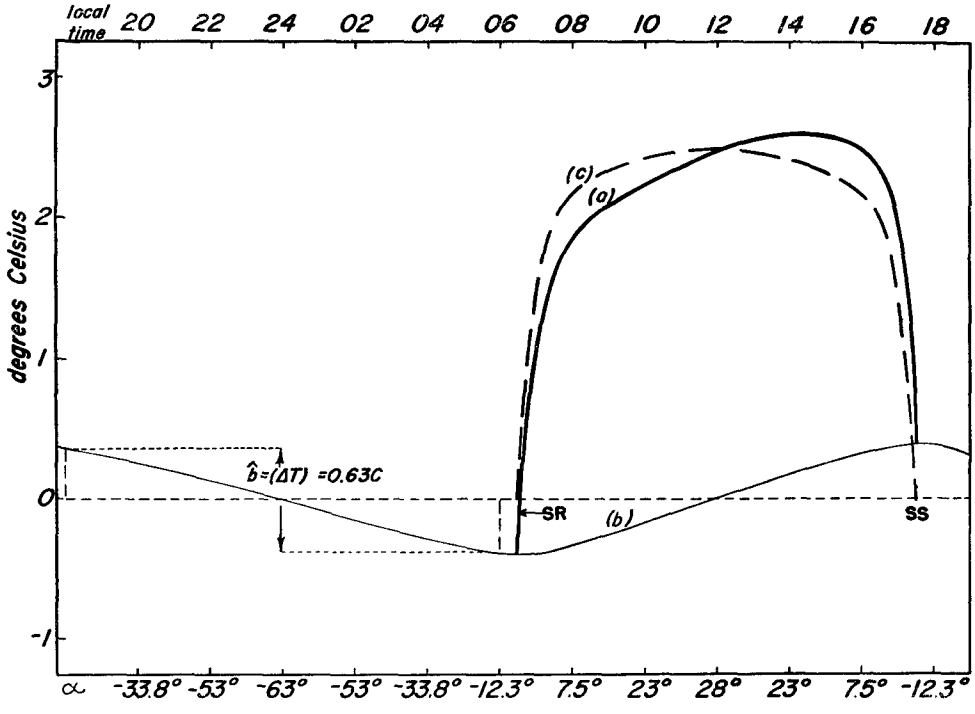

FIG. 14. Model of wintertime temperature variation for 10 mb, 45N.

departures $\pm 0.5\hat{b}$ from this mean. Part of the necessary justification for this procedure is found by reference to the double-darkness analyses (see, e.g., Fig. 7), which show essentially straight horizontal lines of analyzed $\overline{\Delta T}$. Because wintertime darkness at 45N is about 14 hr long, 12-hr differences can be taken over different portions of the night. The near-equality of these differences strongly suggests that the portion of the diurnal variation curve corresponding to nighttime has a constant slope. Therefore, the maximum temperature must occur at the beginning of the period, and the minimum at the end (near sunset and sunrise, respectively). This suggestion of a constant nighttime slope is strengthened by results for 70–80N (Figs. 8 and 10), where the greater length of periods of darkness have permitted a more complete sampling of the temperature curves. A definitive justification for placing the horizontal axis of the model (Figs. 13 and 14) in the manner indicated can be given only after the daytime portion of curve (b) has been delineated.

The day-night difference curves of Fig. 12 provide information which is essential to constructing the daytime portion of curve (b). These curves have been obtained by analyzing data from most of North America, from all seasons, and so cannot be considered representative of any particular station. Nevertheless, the vertical distance between the curves at any given solar elevation angle α must be a measure of the average temperature change between the morning occurrence of α and the afternoon occurrence of α (because the solar error is the same at both times and thus cancels out). An inspection of the curves in Fig. 12 reveals that the vertical distance between them is greatest at low solar angles and tends to decrease as the angles increase. Such a configuration suggests that the true diurnal range is greatest between points of time near sunrise and sunset, and decreases rather uniformly as the time interval (centered at noon) decreases.

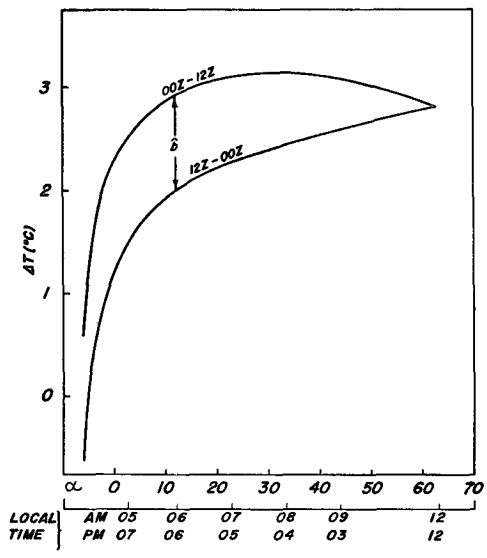

FIG. 15. Average summertime 12-hr day-night temperature differences at 10 mb, 45N. Upper curve represents afternoon-night differences, lower curve morning-night differences.

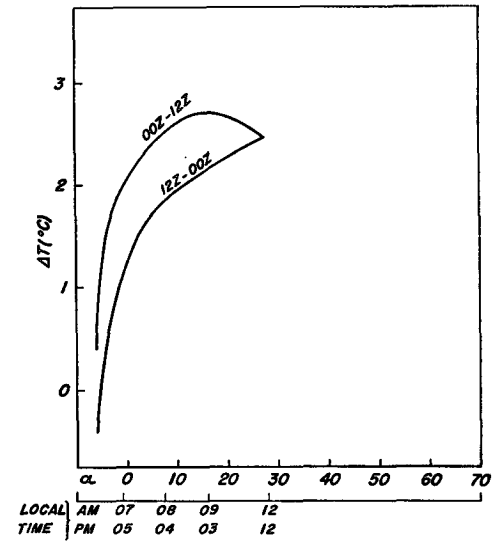

FIG. 16. Same as Fig. 15 except for winter.

In order to employ the curves of day-night temperature differences for the construction of the models shown in Figs. 13 and 14, it is necessary to adjust them according to season and latitude.

Fig. 15 shows the adjusted curves representative of summer, Fig. 16 those representative of winter, for 45N. The adjustments are generally substantiated by a portion of the day-night data sample which includes data taken between the vernal and autumnal equinoxes at stations located in the latitude band from 40–50N. The distance between these curves at a solar angle of 12.3° should be approximately equivalent to the summertime $\hat{b}$ computed for 45N. Continuity requires the curves to merge at noon (since, e.g., the temperature difference between 1100 and 1300 LST must be less than that between 1000 and 1400 LST).

The adjusted day-night difference curves for summer and winter may be shown as the continuous curves (a) on the respective models (Figs. 13 and 14). The portions to the left of local noon represent the morning daylight-night curves and to the right of that point the afternoon daylight-night curves. Analyses of day-night data at low solar angles definitely indicate that the temperatures in the mean are lower in very early morning sunlight than during the early nighttime hours. Also, the temperatures in late afternoon daylight are higher than in early morning darkness. Thus, curve (a) in each section of the model is shown to begin at the minimum of the diurnal curve and end at the maximum value.

A comparison may be made to illustrate the consistency of the day-night curve (a) with the analyzed double-daylight curve (Fig. 4). In order to accomplish this, temperature differences have been extracted from curve (a), as well as the differences between correspond-

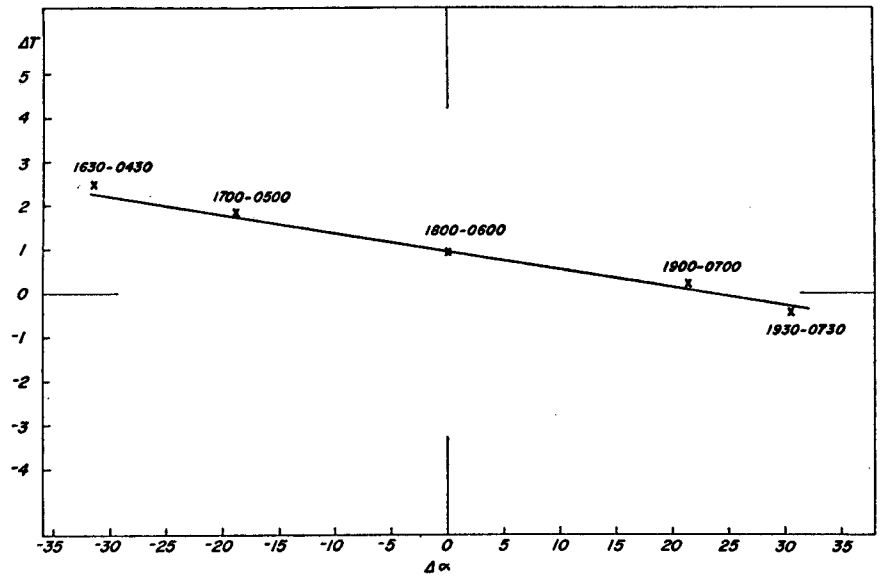

FIG. 17. 12-hr temperature differences from curve (a) of Fig. 13 represented as cross marks; local times used for deriving ΔT values are shown above cross marks. The straight line represents the analysis of the double-daylight scatter diagram for 10 mb, 45N (Fig. 4).

ing solar elevation angles; they are identified in Fig. 13 as representative of western stations (W), central stations (C), and eastern stations (E) (see also Fig. 11). The value of $\hat{b}$ has already been taken into account in the construction of a portion of curve (a). However, other differences obtained from curve (a) are independent of this value of $\hat{b}$, and they are shown in Fig. 17 to be in good agreement with the analysis of the double-daylight data of Fig. 4.

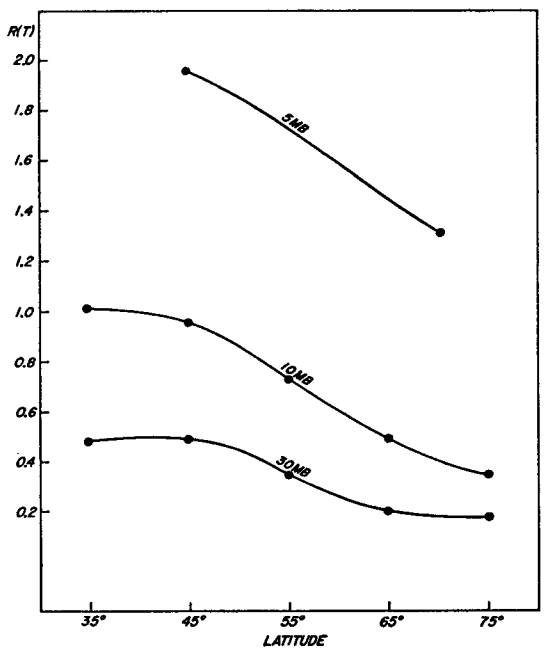

FIG. 18. Summertime variation of diurnal temperature range $R(T)$ for 30, 10 and 5 mb as a function of latitude.

All of the evidence presented suggests rather strongly that the true diurnal temperature change peaks near sunset and has a minimum near sunrise. The values of $\hat{b}$ should closely approximate the range between extremes of this variation, and inflection points in the curve occur near noon and midnight.

Curve (c) on the model, derived by subtracting curve (b) from curve (a), is taken to be the curve of solar radiation error. As one would expect, considering that the solar error is a function exclusively of solar elevation angle, curve (c) is symmetric with respect to local noon. The effect of infrared radiation does not appear in this model; however, since it is taken to be essentially constant throughout the diurnal period, it could only result in a shifting of the base-line.

7. Variations of diurnal range with height and latitude

The computed estimates of the diurnal temperature range $R(T)$ (given as $\hat{b}$ in Tables 1 and 2) show a definite increase with altitude[3] (Figs. 18 and 19). During summer, the indicated diurnal temperature range at 5 mb is $2\text{–}\frac{1}{2}$ times that at 10 mb, and in turn that at 10 mb is double that at 30 mb. In winter the change with height is not so clearly defined. Changes of $R(T)$ with latitude are also evident, especially in summer, when the decrease with increasing latitude is quite smooth. However, latitudinal variation during winter is rather ill-defined. At 30 mb, the temperature variation is less than 0.4C and generally decreases with latitude. No definite explanation can be given for the seemingly

[3] One may see, by examining the 95%-confidence intervals listed in Tables 1 and 2, that $R(T)$ is not as well determined at some latitudes as at others.

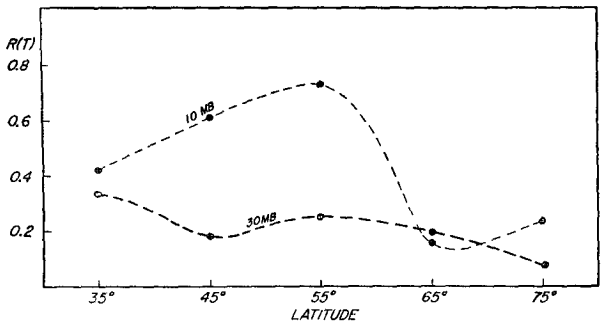

FIG. 19. Same as Fig. 18 except for winter, and omitting the 5-mb level.

strange behavior of the 10-mb curve. This may be due in part to the size of the data sample, which is considerably smaller than that upon which the double-daylight analyses are based. It is interesting to speculate that the curve may give some indication of atmospheric behavior at 10 mb. Leovy (1964), for example, has presented evidence that the ozone concentration at this level during the winter increases slightly with increasing latitude south of 50N, but decreases sharply north of 50N. Whatever the ozone distribution, it seems clear that above the Arctic Circle in winter very little sunlight penetrates into the ozone layer to produce periodic heating. However, dynamical effects induced by daily variations at low latitudes must also be considered in any explanation for the variation of $R(T)$ with latitude.

Fig. 20 indicates how well the values of $\hat{b}$ agree with some results of Leovy (1964) and Lindzen (1967). There is also rather good agreement with the results of Harris *et al.* (1962) and of Hering *et al.* (1967).

8. Conclusions

The general use of a single type of radiosonde instrument within much of North America, in addition to the unique seasonal variability in times of sunrise and sunset with respect to standard rawinsonde observation times, has made possible an empirical determination of the diurnal temperature variation and shortwave instrumental error at levels within the middle stratosphere. Means of 12-hr temperature differences taken under conditions of double-daylight, double-darkness, and daylight-darkness provided sufficient information for the construction of a basic model which separates the real from the spurious perturbation. The indicated real diurnal temperature variation reaches a maximum near sunset and a minimum near sunrise. The amplitude of this variation clearly increases with altitude between the 30- and 5-mb levels and is found to be dependent on latitude. A seasonal effect is strongly suggested.

Ideally, a study of diurnal variation would utilize a data sample of frequent observations throughout the daily period. Until such a data-sample is available, and

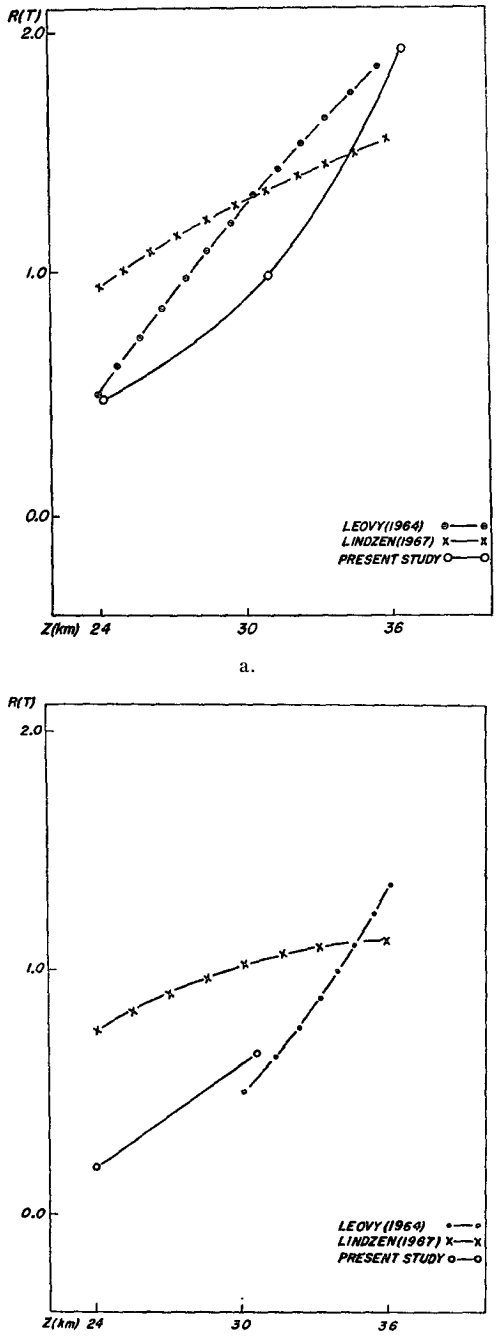

FIG. 20. Estimates of $R(T)$ at 45N for summer, a., and winter, b.

until uncertainties in instrumental radiation errors are wholly eliminated, the results of the present study provide preliminary, though reasonable, estimates of the diurnal variation. There is a need for further studies of the infrared component of instrumental error, in order to test more thoroughly the working hypothesis that this component does not have an appreciable mean diurnal variation (in comparison with other factors).

A further step in continuing the line of research reported in this paper would consist in performing analyses of data over shorter time intervals, in order to delineate a month-by-month trend in the diurnal stratospheric temperature variation. Of principal interest would be the correlation of such a trend with the distribution of various stratospheric constituents, notably ozone, as well as the changes in radiation incident on the instrument, caused, for example, by clouds and snow cover.

Acknowledgments. The research upon which this paper is based was sponsored in part by the U. S. Navy, Naval Air Systems Command. Funds were also provided by the National Science Foundation. The authors are grateful to Gerald F. Cotten for his valuable assistance in the statistical analysis of our data, and to J. Gary Ament for his work in the early phases of the project.

REFERENCES

Badgley, F. I., 1957: Response of radiosonde thermistors. *Rev. Sci. Instr.*, **28**, 1079–1084.

Barr, W. C., 1961: Theoretical considerations in the design of atmospheric temperature-sensing elements. U. S. Army Signal Res. & Develop. Lab., Tech. Rept. 2195 (ASTIA AD 255896), 15 pp.

Finger, F. G., R. B. Mason and S. Teweles, 1964: Diurnal variation in stratospheric temperatures and heights reported by the U. S. Weather Bureau outrigger radiosonde. *Mon. Wea. Rev.*, **92**, 243–250.

——, M. F. Harris and S. Teweles, 1965a: Diurnal variation of wind, pressure, and temperature in the stratosphere. *J. Appl. Meteor.*, **4**, 632–635.

——, H. M. Woolf and C. E. Anderson, 1965b: A method for objective analysis of stratospheric constant-pressure charts. *Mon. Wea. Rev.*, **93**, 619–638.

Harris, M. F., 1959: Diurnal and semidiurnal variations of wind, pressure and temperature in the troposphere at Washington, D. C. *J. Geophys. Res.*, **64**, 983–995.

——, F. G. Finger and S. Teweles, 1962: Diurnal variations of wind, pressure, and temperature in the troposphere and stratosphere over the Azores. *J. Atmos. Sci.*, **19**, 136–149.

Hering, W. S., C. N. Touart and T. R. Borden, Jr., 1967: Ozone heating and radiative equilibrium in the lower stratosphere. *J. Atmos. Sci.*, **24**, 402–413.

Kuhn, P. M., and S. K. Cox, 1968: Convective heat transfer at surfaces of an ascending radiation sonde. Environmental Sciences Services Admin., unpublished manuscript.

Leovy, C., 1964: Radiative equilibrium of the mesosphere. *J. Atmos. Sci.*, **21**, 238–248.

Lindzen, R. S., 1967: Thermally driven tide in the atmosphere. *Quart. J. Roy. Meteor. Soc.*, **93**, 18–42.

Ney, E. P., R. W. Maas and W. F. Huch, 1961: The measurement of atmospheric temperature. *J. Meteor.*, **18**, 60–80.

Pressman, J., 1955: Diurnal temperature variations in the middle atmosphere. *Bull. Amer. Meteor. Soc.*, **36**, 220–223.

Rao, P. K., E. G. Astling and F. S. Winninghoff, 1965: An investigation of degradation errors in the TIROS IV scanning radioeter data and the determination of correction factors. Meteor. Satellite Lab., Rept. No. 34 (manuscript), ESSA, Washington, D. C., 22 pp.

Teweles, S., 1963: Reduction of diurnal variation in stratospheric radiosonde data reported by some countries of the Eastern Hemisphere. *Meteor. Abhandl.*, **36**, 507–516.

——, and F. G. Finger, 1960: Reduction of diurnal variation in the reported temperatures and heights of stratospheric constant-pressure surfaces. *J. Meteor.*, **17**, 177–194.